Article

Copyright © 2016 American Scientific Publishers
All rights reserved
Printed in the United States of America

Journal of
Nanoscience and Nanotechnology
Vol. 16, 10841–10845, 2016
www.aspbs.com/jnn

Hydrogenation of Succinic Acid to Tetrahydrofuran Over Ruthenium–Carbon Composite Catalyst: Effect of Catalyst Preparation Condition

Ung Gi Hong, Ki Hyuk Kang, Ji Hwan Song, Tae Hyeop Kim, and In Kyu Song*

School of Chemical and Biological Engineering, Institute of Chemical Processes, Seoul National University,
Shinlim-dong, Kwanak-ku, Seoul 151-744, South Korea

Ruthenium–carbon composite (Ru–C-*X*) catalysts were prepared by a single-step surfactant-templating method at different sucrose/P123 molar ratio ($X = 3$, 5, 7, 9, 11, and 15). Ru–C-*X* ($X = 3$, 5, 7, 9, 11, and 15) catalysts were characterized by BET, nitrogen adsorption–desorption isotherm, XRD, and HR-TEM analyses. Liquid-phase hydrogenation of succinic acid to tetrahydrofuran (THF) was carried out over Ru–C-*X* catalysts in a batch reactor. The effect of sucrose/P123 molar ratio on the physicochemical properties and catalytic activities of Ru–C-*X* catalysts ($X = 3$, 5, 7, 9, 11, and 15) was investigated. It was revealed that Ru–C-*X* composite catalysts showed different ruthenium particle size depending on sucrose/P123 molar ratio. Characterization results showed that an optimal sucrose/P123 molar ratio was required to achieve fine dispersion of ruthenium in the Ru–C-*X* catalysts. Yield for THF in the hydrogenation of succinic acid increased with decreasing average ruthenium particle size of Ru–C-*X* catalysts. Ruthenium particle size served as an important factor determining the catalytic performance of Ru–C-*X* in the hydrogenation of succinic acid to THF. Among the catalysts tested, Ru–C-9 with the smallest ruthenium particle size showed the highest yield for THF.

Keywords: Succinic Acid, Tetrahydrofuran, Ru–C Composite Catalyst, Mesoporous Carbon.

1. INTRODUCTION

Tetrahydrofuran (THF) is an important raw material in various polymer industries. THF can be converted into polytetramethylene ether glycol (PTMEG), thermoplastic polyesters, and polyurethane elastomers.[1–3] THF is also widely used as a solvent in paint industries. THF is traditionally produced via several industrial routes such as oxidative hydrogenation of maleic anhydride (MAN), acid-catalyzed dehydration of 1,4-butanediol (BDO), hydroformylation of ally alcohol, and oxidation of butadiene (BD).[4–6] Because all these feedstocks (MAN, BDO, ally alcohol, and BD) are petrochemicals, the traditional THF production processes lead to several problems such as unstable price and environmental issue. Therefore, demands for finding an eco-friendly feedstock that can solve these problems have continuously increased.

Recently, succinic acid (SA) has attracted much attention as a cheap and bio-derived chemical that can be converted into THF.[7–10] It is known that ruthenium is an efficient catalyst in the hydrogenation of succinic acid to THF, while carbon serves as an excellent supporting material for ruthenium.[11–14] Many researches on ruthenium catalyst supported on carbon have been focused on increasing ruthenium dispersion via carbon support modification.

It has been reported that structure of carbon framework prepared using a self-assembled block copolymer can be controlled by changing carbon precursor/block copolymer ratio.[15,16] In one-pot surfactant-templating method (metal-carbon composite system), in particular, structure of mesoporous carbon is very important to increase metal dispersion, because metal particle size of metal-carbon composite can be controlled by changing carbon precursor/block copolymer ratio. If metal-carbon composite is prepared to have controllable ruthenium dispersion, therefore, it can serve as an excellent catalyst in the hydrogenation of succinic acid with high catalytic activity. Furthermore, metal-carbon

---

*Author to whom correspondence should be addressed.

1533-4880/2016/16/10841/005 doi:10.1166/jnn.2016.13250

composite prepared by an one-pot surfactant-templating method provides a simple preparation route.

In this work, ruthenium–carbon composite (Ru–C-X) catalysts were prepared by an one-pot surfactant-templating method at different sucrose/block copolymer molar ratio ($X = 3, 5, 7, 9, 11,$ and 15) to control the structure of ruthenium–carbon composite, i.e., to control the ruthenium dispersion. The Ru–C-X catalysts were characterized by BET, N_2 adsorption–desorption isotherm, XRD, and HR-TEM analyses. Liquid-phase hydrogenation of succinic acid to THF was performed over Ru–C-X catalysts in a batch reactor. The effect of sucrose/block copolymer molar ratio on the physicochemical properties and catalytic activities of ruthenium–carbon composite (Ru–C-X) catalysts was examined.

2. EXPERIMENTAL DETAILS

2.1. Preparation of Ruthenium–Carbon Composite Catalyst (Ru–C-X)

Known amounts of sucrose (3.2, 5.1, 6.6, 8.0, 9.2, and 11.3 g) (Aldrich) and surfactant (18.3, 17.1, 16.0, 15.0, 14.1, and 12.8 g) (P123, Aldrich) were dissolved in 5 M HCl solution (300 ml) with ruthenium precursor ($RuCl_3$, 1.27 g, Kojima Chemical) at 40 °C for 4 h under stirring. After silica precursor (TEOS, 36 ml, Aldrich) and 0.4 M of H_2SO_4 (10 ml) were slowly added into the solution, the mixture was constantly stirred for 3 h. After the mixture was dried at 100 °C for 48 h, the resulting brown powder was carbonized at 800 °C for 4 h at a heating rate of 5 °C/min under a nitrogen stream (100 ml/min). The resultant was further treated with 5 wt% HF solution to remove silica template. The dried ruthenium–carbon composite was then reduced with a mixed stream of hydrogen (2.5 ml/min) and nitrogen (47.5 ml/min) at 450 °C prior to characterization and catalytic reaction. The ruthenium–carbon composite catalysts prepared at different sucrose/P123 molar ratio (3, 5, 7, 9, 11, and 15) were denoted as Ru–C-X, where X represented sucrose/P123 molar ratio.

2.2. Characterization

Nitrogen adsorption–desorption isotherms of ruthenium–carbon composite (Ru–C-X, $X = 3$, 5, 7, 9, 11, and 15) catalysts were obtained with an ASAP-2010 instrument (Micromeritics). Surface areas and pore volumes of the catalysts were calculated using the BET equation and the BJH model, respectively. Crystalline state and ruthenium particle size of Ru–C-X ($X = 3$, 5, 7, 9, 11, and 15) catalysts were examined by XRD measurements. XRD patterns of Ru–C-X ($X = 3$, 5, 7, 9, 11, and 15) catalysts were obtained with a Rigaku D-Max2500-PC instrument using Cu–Kα radiation ($\lambda = 1.541$ Å) operated at 50 kV and 100 mA. Ruthenium particle size and ruthenium dispersion were examined by CO chemisorption (BELCAT-B, BEL Japan) and HR-TEM (Jeol, JEM-3000F) analyses.

2.3. Hydrogenation of Succinic Acid

Liquid-phase hydrogenation of succinic acid (SA) to THF was carried out over Ru–C-X ($X = 3$, 5, 7, 9, 11, and 15) catalysts in a batch reactor at 240 °C and 80 bar (H_2). Succinic acid (0.5 g) and a reduced Ru–C-X catalyst (0.2 g) were charged into an autoclave (150 ml). 1,4-Dioxane (50 ml) was used as a solvent for the reaction. The reactor was purged with nitrogen to remove air, and then it was pressurized up to 40 bar using hydrogen. After heating the reactor to reaction temperature (240 °C), hydrogen pressure was raised up to 80 bar. The catalytic reaction was carried out for 4 h. During the reaction, reaction mixture was stirred at 500 rpm in order to avoid mass transfer limitation. Reaction products were analyzed using a gas chromatograph (Younglin, ACME-6100) equipped with a FID (flame ionization detector).

3. RESULTS AND DISCUSSION

3.1. Physicochemical Properties of Ru–C-X Catalysts

Figure 1 shows the nitrogen adsorption–desorption isotherms of Ru–C-X ($X = 3$, 5, 7, 9, 11, and 15) catalysts reduced at 450 °C. All the Ru–C-X catalysts exhibited type-IV isotherm with type-H3 or type-H4 hysteresis loop, indicating the existence of mesopores.[17, 18] With increasing sucrose/P123 molar ratio of Ru–C-X ($X = 3$, 5, 7, and 9) catalysts, type-H4 hysteresis loop was transformed to more apparent type-H3 hysteresis loop. In the Ru–C-X ($X = 9$, 11, and 15) catalysts, however, type-H3 hysteresis gradually disappeared with increasing sucrose/P123 molar ratio. Textural properties of Ru–C-X ($X = 3$, 5, 7, 9, 11, and 15) catalysts reduced at 450 °C are summarized in Table I. Average pore size of Ru–C-X catalysts was in the mesopore range (3.7–5.1 nm). BET surface area and average pore volume of Ru–C-X showed a volcano-shaped trend with respect to sucrose/P123 molar ratio. BET surface area and average pore volume of Ru–C-X ($X = 3$,

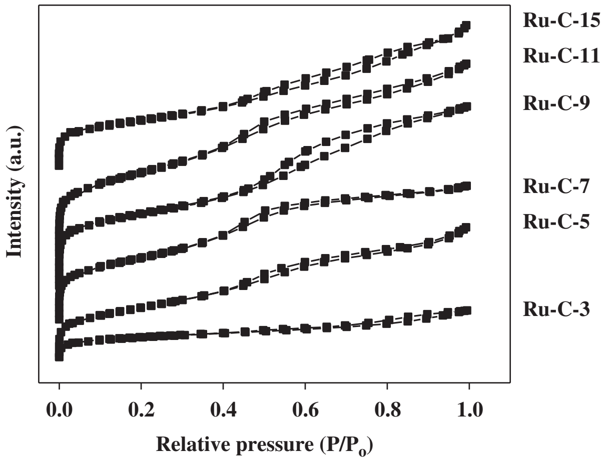

Figure 1. Nitrogen adsorption–desorption isotherms of Ru–C-X catalysts reduced at 450 °C.

Table I. Physicochemical properties of Ru–C-X catalysts.

	Surface area (m^2/g-cat.)	Pore volume (cm^3/g-cat.)	Average pore size (nm)	Ru particle size		
				By XRD	By HR-TEM	By CO chemisorption
Ru–C-3	252	0.23	3.7	20.9	24.3	32.4
Ru–C-5	958	0.89	3.7	8.9	10.4	11.7
Ru–C-7	1016	0.93	3.8	4.2	5.9	5.4
Ru–C-9	1367	1.38	4.0	3.2	4.1	3.9
Ru–C-11	1082	1.19	4.4	3.8	5.3	4.2
Ru–C-15	672	0.85	5.1	16.3	18.7	23.5

5, 7, and 9) increased with increasing sucrose/P123 molar ratio due to the increase of carbon framework formation between sucrose and P123. In the Ru–C-X ($X = 9, 11$, and 15) catalysts, on the other hand, BET surface area and average pore volume decreased due to the excess amount of sucrose precursor. These results indicate that there is an optimal sucrose/P123 ratio to form well-developed mesoporous structure of carbon framework.

3.2. Crystalline State and Ruthenium Dispersion of Ru–C-*X* Catalysts

Figure 2 shows the XRD patterns of Ru–C-X ($X = 3$, 5, 7, 9, 11, and 15) catalysts reduced at 450 °C. All the reduced Ru–C-X catalysts showed a weak shoulder at $2\theta = 25°$, which was attributed to graphitic carbon.[19] All the reduced Ru–C-X catalysts exhibited no XRD peaks of ruthenium oxide but showed XRD peaks of metallic ruthenium at $2\theta = 44°$.[20] This result indicates that ruthenium species in the Ru–C-X catalysts were completely reduced into metallic ruthenium during the reduction process.

It was also observed that ruthenium peak intensity of Ru–C-X catalysts decreased in the order of Ru–C-3 > Ru–C-15 > Ru–C-5 > Ru–C-7 > Ru–C-11 > Ru–C-9. This result indicates that ruthenium in the Ru–C-9 catalyst was most finely dispersed on the carbon framework. In order to determine the accurate dispersion of ruthenium in the Ru–C-X catalysts, particle size of ruthenium was calculated from XRD patterns using the Debye-Scherrer equation[21] and CO chemisorption.

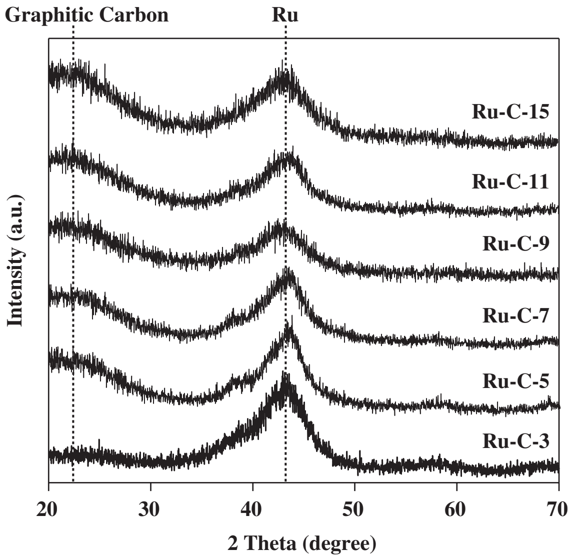

Figure 2. XRD patterns of Ru–C-X catalysts reduced at 450 °C.

Table I shows the average ruthenium particle sizes of Ru–C-X catalysts determined by XRD and CO chemisorption measurements. Ruthenium particle sizes of Ru–C-X catalysts determined by XRD and CO chemisorption measurements showed the same trend with respect to sucrose/P123 molar ratio. In the Ru–C-X ($X = 3, 5, 7$, and 9) catalysts, ruthenium particle size became smaller with increasing sucrose/P123 molar ratio. In the Ru–C-X ($X = 9, 11$, and 15) catalysts, however, ruthenium particle size increased with increasing sucrose/P123 molar ratio. These might be explained by difference in mesoporosity, as observed for the trends of BET surface area and average pore volume of Ru–C-X catalysts with respect to sucrose/P123 molar ratio. Because metal nanoparticles tend to aggregate, it is important to form high surface area and large pore volume for fine dispersion of ruthenium in the ruthenium–carbon composite material. Thus, an optimal sucrose/P123 molar ratio ($X = 9$) was required to yield small ruthenium particles in the Ru–C-X catalysts.

Figure 3 shows the HR-TEM images of Ru–C-X ($X = 3$, 5, 7, 9, 11, and 15) catalysts reduced at 450 °C. In the Ru–C-X ($X = 3, 5, 7$, and 9) catalysts, ruthenium particle size became smaller with increasing sucrose/P123 molar ratio. In the Ru–C-X catalysts ($X = 9, 11$, and 15), however, ruthenium particle size became larger with increasing sucrose/P123 molar ratio. In order to determine the ruthenium particle size of Ru–C-X catalysts from HR-TEM images, sizes of 200 metallic ruthenium particles in the reduced catalysts were directly measured as also summarized in Table I. It was observed that the trend of average ruthenium particle size determined by HR-TEM was well consistent with the trend of ruthenium particle size determined by XRD and CO chemisorption. Among the Ru–C-X catalysts, Ru–C-9 catalyst showed the smallest ruthenium particle size (less than 5 nm) while Ru–C-3 catalyst showed the largest ruthenium particle size (above 20 nm).

3.3. Hydrogenation of Succinic Acid to THF Over Ru–C-*X* Catalysts

Catalytic performance of Ru–C-X ($X = 3$, 5, 7, 9, 11, and 15) catalysts in the liquid-phase hydrogenation of succinic acid to THF is shown in Figure 4. THF and γ-butyrolactone (GBL) were mainly produced via consecutive hydrogenation of succinic acid. Ethanol was produced as a major by-product via side reaction of succinic acid, and small amounts of acids (acetic acid, butyric acid, and propionic acid) were also produced as by-products.

As shown in Figure 4, yield for THF showed a volcano-shaped trend with respect to sucrose/P123 molar ratio.

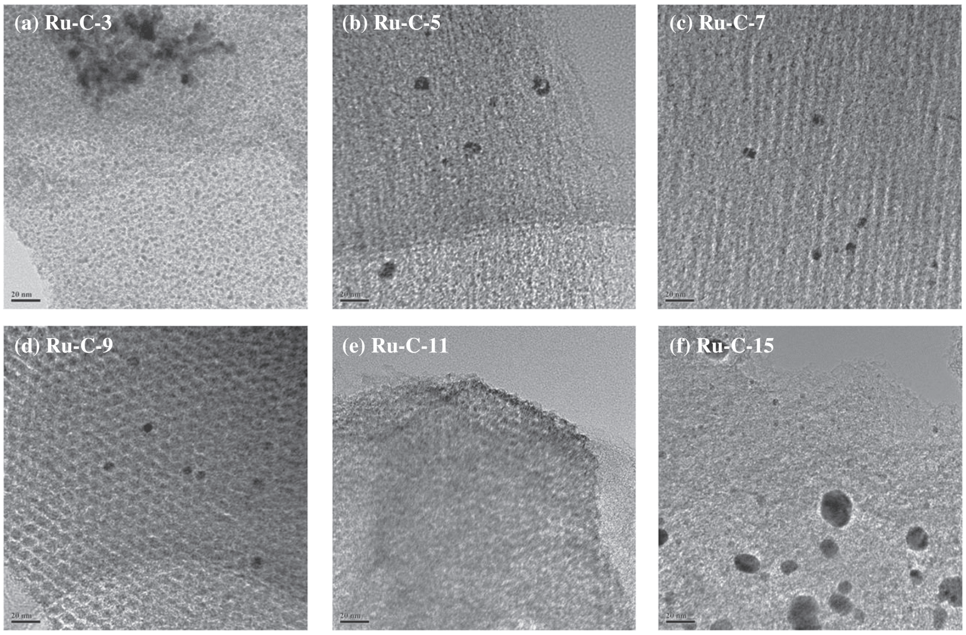

Figure 3. HR-TEM images of Ru–C-*X* catalysts reduced at 450 °C.

This means that an optimal sucrose/P123 molar ratio was required for maximum production of THF. Among the catalyst tested, Ru–C-9 catalyst showed the highest yield for THF (45.3%), while Ru–C-3 catalyst showed the lowest yield for THF (12.1%). It is believed that the excellent catalytic performance of Ru–C-9 catalyst was due to fine dispersion of ruthenium.

In order to investigate the effect of ruthenium dispersion of Ru–C-X ($X = 3$, 5, 7, 9, 11, and 15) catalysts on the catalytic activity in the hydrogenation of succinic acid, a correlation between average ruthenium particle size of Ru–C-*X* catalysts and yield for THF was established. Figure 5 shows the correlation between ruthenium particle size of Ru–C-*X* catalysts (determined by HR-TEM) and yield for THF in the hydrogenation of succinic acid. The correlation clearly showed that yield for THF increased with decreasing ruthenium particle size (with increasing ruthenium dispersion) of Ru–C-*X* catalysts. This result strongly supports that ruthenium particle size of Ru–C-*X* catalysts served as a key factor determining the catalytic performance in the hydrogenation of succinic acid to THF.

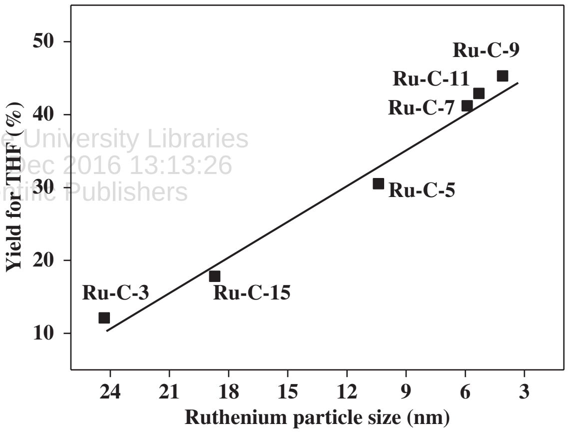

Figure 5. A correlation between ruthenium particle size (determined by HR-TEM) and catalytic activity of Ru–C-*X* catalysts in the hydrogenation of succinic acid to THF.

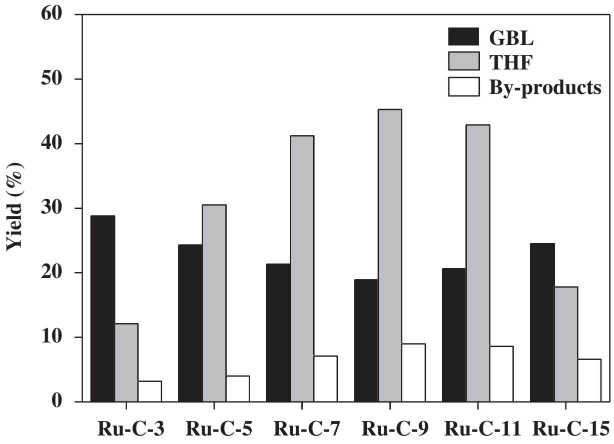

Figure 4. Catalytic performance of Ru–C-*X* catalysts.

4. CONCLUSIONS

Ruthenium–carbon composite (Ru–C-*X*) catalysts were prepared by a single-step surfactant-templating method at different sucrose/P123 molar ratio ($X = 3$, 5, 7, 9, 11, and 15) to control the ruthenium dispersion of Ru–C-*X* catalysts. They were then applied to the liquid-phase hydrogenation of succinic acid to THF. Among the Ru–C-*X* ($X = 3$, 5, 7, 9, 11, and 15) catalysts, Ru–C-9 catalyst showed the smallest ruthenium particle size due to well-developed mesoporous structure. In the hydrogenation of succinic acid, yield for THF showed a volcano-shaped trend with respect to sucrose/P123 molar ratio. Thus, an optimal sucrose/P123 molar ratio in the preparation of Ru–C-X composite catalysts was required to achieve maximum yield for THF. Yield for THF in the hydrogenation of succinic acid increased with decreasing ruthenium particle size of Ru–C-*X* catalysts. Ruthenium particle size (ruthenium dispersion) played a key role in determining the catalytic performance in the hydrogenation of succinic acid to THF over Ru–C-*X* catalysts.

Acknowledgments: This work was supported by the Global Frontier R&D Program on Center for Multiscale Energy System funded by the National Research Foundation under the Ministry of Science, ICT and Future Planning, Korea (20110031575).

References and Notes

1. A. Küksal, E. Klemm, and G. Emig, *App. Catal. A: Gen.* 228, 237 (**2002**).
2. J. A. F. F. Rocco, J. E. S. Lima, V. L. Lourenco, N. L. Batista, E. C. Botelho, and K. Iha, *J. Appl. Polym. Sci.* 126, 1461 (**2012**).
3. S. P. Müller, M. Kucher, C. Ohlinger, and B. Kraushaar-Czarnetzkyi, *J. Catal.* 218, 419 (**2003**).
4. Y. Feng, H. Yin, A. Wang, T. Xie, and T. Jiang, *Appl. Catal. A:Gen.* 425–426, 205 (**2012**).
5. Q. Zhang, Y. Zhang, H. Li, C. Gao, and Y. Zhao, *Appl. Catal. A:Gen.* 466, 233 (**2013**).
6. M. D. Wildberger, M. Maciejewski, J.-D. Grunwaldt, T. Mallat, and A. Baiker, *Appl. Catal. A:Gen.* 179, 189 (**1999**).
7. H. Choudhary, S. Nishimura, and K. Ebitani, *Appl. Catal. A:Gen.* 458, 55 (**2013**).
8. C. Delhomme, D. Weuster-Botz, and F. E. Kühn, *Green Chem.* 11, 13 (**2009**).
9. A. Cukalovic and C. V. Stevens, *Biofuels Bioprod. Biorefin.* 2, 505 (**2008**).
10. B. Tapin, F. Epron, C. Especel, B. K. Ly, C. Pinel, and M. Besson, *ACS Catal*. 3, 2327 (**2013**).
11. L. Rosi, M. Frediani, and P. Frediani, *J. Org. Chem.* 695, 1314 (**2010**).
12. R. Luque and J. H. Clark, *Catal. Commun*. 11, 928 (**2010**).
13. R. M. Deshpande, V. V. Buwa, C. V. Rode, R. V. Chaudhari, and P. L. Mills, *Catal. Commun.* 3, 269 (**2002**).
14. U. G. Hong, H. W. Park, J. Lee, S. Hwang, J. Yi, and I. K. Song, *Appl. Catal. A:Gen.* 415–416, 141 (**2012**).
15. S. Tanaka, N. Nishiyama, Y. Egashira, and K. Ueyama, *Chem. Commun.* 2125 (**2005**).
16. S. Tanaka, Y. Katayama, M. P. Tate, H. W. Hillhouse, and Y. Miyake, *J. Mater. Chem*. 17, 3639 (**2007**).
17. K. S. W. Sing, D. H. Everett, R. A. W. Haul, L. Moscou, R. A. Pierotti, J. Rouquérol, and T. Siemieniewska, *Pure Appl. Chem.* 57, 602 (**1985**).
18. S. Lu and Y. Liu, *Appl. Catal. B: Environ.* 111–112, 492 (**2012**).
19. Z. Q. Li, C. J. Lu, Z. P. Xia, Y. Zhou, and Z. Luo, *Carbon* 45, 1686 (**2007**).
20. Z.-Z. Lin, T. Okuhara, and M. Misono, *J. Phys. Chem.* 92, 723 (**1988**).
21. Q. Li, B. Guo, J. Yu, J. Ran, B. Zhang, H. Yan, and J. R. Gong, *J. Am. Chem. Soc.* 133, 10878 (**2011**).

Received: 3 July 2015. Accepted: 4 February 2016.